PROCEEDINGS OF SCIENCE

Probing neutrino yield from different gamma-ray burst populations using the entire ANTARES data set

Marco Scarnera,[a,b,*] **Gwenhaël de Wasseige,**[a] **Antoine Kouchner**[b,c] **and Mathieu Lamoureux**[a] **on behalf of the ANTARES collaboration**

[a] *Centre for Cosmology, Particle Physics and Phenomenology - CP3, Universite Catholique de Louvain, B-1348 Louvain-la-Neuve, Belgium*

[b] *Astroparticule et Cosmologie - APC, Université Paris Cité, 10 Rue Alice Domon et Léonie Duquet, 75013 Paris, France*

[b] *Institut Universitaire de France, 1 rue Descartes, 75005 Paris, France*

E-mail: marco.scarnera@uclouvain.be, kouchner@apc.in2p3.fr, gwenhael.dewasseige@uclouvain.be, mathieu.lamoureux@uclouvain.be

While the evidence of high-energy neutrinos was established a decade ago and confirmed independently by the observation of an ultra-high-energy neutrino recently announced, the origin of these neutrinos is not yet fully identified. Gamma-ray bursts (GRBs) have long been one of the most promising candidate emitters of such neutrinos. Despite not having led to a significant detection in neutrinos so far, the observations were focusing on GRBs that were bright in gamma rays. Dividing the GRBs detected so far into various subpopulations based on their signal in gamma rays and searching for neutrinos from each of the subpopulations separately may lead to more relevant constraints on the sources. The ANTARES telescope offers a great opportunity to test this assumption because of the more than 15 years of data that were collected. In this contribution, we present the sensitivity to different subpopulations of GRBs and describe the various efforts that will lead to the first catalogue of neutrino constraints from GRBs.

39th International Cosmic Ray Conference (ICRC2025)
15–24 July 2025
Geneva, Switzerland

ICRC 2025
The Astroparticle Physics Conference
Geneva July 15-24, 2025

*Speaker

PoS(ICRC2025)1167

1. Introduction

A decade ago, the discovery of an astrophysical neutrino flux at high energies was reported by the IceCube Collaboration [1], recently corroborated by the observation of an ultra-high-energy neutrino from the KM3NeT experiment [2]. Understanding the origin of this flux represents one of the main goals of the current astroparticle physics community. The search is directed toward sources that can explain the observed high energies, and several possible sources have been identified by IceCube in recent years [3–5]. Different classes of progenitors are considered and, searching among the most powerful accelerators that can explain the observed neutrino energies and that could also be sources of Ultra-High-Energy Cosmic Rays (UHECR), Gamma-Ray Bursts (GRBs) are among the most promising candidates. GRBs are short bursts of gamma radiation occurring a few times per day in the detectable Universe and releasing a vast amount of energy, between 10^{50} and 10^{54} erg. GRBs are also events of particular interest as they were the leading actors of the new era of multi-messenger astrophysics, with the 2017 observation of GW170817, a gravitational wave (GW) signal from a neutron star merger event, followed by the GRB170817A Gamma-Ray Burst [6]. This event represented the first clear identification of an electromagnetic counterpart to a gravitational wave event. Many details remain unresolved about the processes underlying these extreme phenomena. Some models describing the formation and evolution of GRBs predict the presence of hadronic processes. Shock-accelerated protons and ions can interact with the intense radiation field of the collimated jet generated in GRBs and, as a result of the photomeson production of pions, generate an associated burst of neutrinos, with a wide range of possible energy values, from MeV to PeV [7].

Neutrinos are ideal messengers for the search and understanding of the processes at the core of these distant astrophysical objects. Being electrically neutral, stable, and weakly interacting particles, they are invisible to the presence of magnetic fields and interstellar matter: their direction of origin is consequently an excellent indicator of the source location. Detecting neutrinos in temporal and spatial coincidence with GRBs would unequivocally identify them as hadronic factories, bring new information about their internal mechanisms and the composition of their jets, and support the hypothesis that GRBs are sources of UHECR.

To detect cosmic neutrinos, very-large neutrino telescopes are needed. The ANTARES neutrino telescope [8], located in the depths of the Mediterranean Sea and operating from 2007 to 2022, was for several years the largest neutrino observatory in the Northern Hemisphere. It consisted of a three-dimensional array of 885 optical modules (OMs) based on photomultiplier tubes (PMTs), distributed over 12 vertical lines and corresponding to an instrumented volume of about 0.015 km^3. The OMs detect the faint Cherenkov light of secondary charged particles produced by neutrino interactions, reconstructing their direction, energy, and flavor. Given the performance and characteristics, the detector is sensitive mainly to neutrinos in the energy range between TeV and PeV. The various analyses looking for neutrinos spatially and temporally coincident with GRBs conducted in recent years by ANTARES [9] and IceCube [10], including the recent search by KM3NeT for neutrinos coincident with the brightest GRB ever observed, i.e., GRB221009A [11], have found no significant association with compatible results among the various experiments. The non-detection, however, has allowed increasingly stringent upper limits to be placed on the contribution of these sources to the diffuse flux and significant constraints on the various theoretical models. In this work, the search for astrophysical neutrinos from GRBs is extended, with respect to the previous searches,

PoS(ICRC2025)1167

including for the first time the entire ANTARES dataset.

2. Analysis method

The presented analysis studies the capabilities of the ANTARES neutrino telescope to detect a high-energy neutrino signal associated with GRBs. The search for astrophysical neutrinos is performed by looking for neutrino events within ±500 seconds from the GRB trigger time. This conservative time window Δt_{GRB} has been derived in [12], taking into account the upper limit of GRB durations as observed by BATSE [13] and bounds on precursor neutrino (and/or GW) emission. The GRB parameters used in the analysis are obtained from the Fermi Gamma-ray Burst Monitor (GBM) catalog [14]. As this study focuses on up-going track-like (i.e., muon) events, the selected GRBs are located below the local horizon for ANTARES, i.e., the events have the reconstructed zenith angle greater than 90°. We require that all the processed events are taken during reliable data collection periods (runs) and that the estimated angular uncertainty on the track direction must be below 1°.

To measure the detector performance in separating presumable signal from background, we optimize the event selection on two different parameters: the track-fit quality Λ and the angular distance α, between the GRB's position and the reconstructed event direction. In this study, the main (and irreducible) background component is represented by atmospheric neutrinos from below the local horizon, while a smaller contribution is characterized by wrongly reconstructed down-going atmospheric muons. Higher values of Λ indicate a higher event reconstruction quality, and therefore a higher suppression of atmospheric muons wrongly reconstructed as up-going events. On the other hand, varying α accounts for the angular spread of events around the burst direction. The value of α, with a baseline at the 1σ error on the GRB position, defines the dimension of our search cone or Region of Interest (RoI).

2.1 Background and signal estimation

For a realistic estimate, the number of background events μ_b is computed from real reconstructed event data. The distribution of background events is assumed to be uniform within a 10° search cone around the position of the GRB, i.e., the maximum dimension of the RoI. The same assumption is adopted for its rate in the 1000-second search time window. Given the small number of up-going events, the dimension of the RoI, and to have a robust estimate, a large sample is needed. This requires averaging the number of background events over large periods and, therefore, over different detector conditions, which are strongly related to seasonal variations of the optical background in seawater. As a consequence, μ_b is assessed by using all runs' data within ±1 year from the GRB trigger, and with a similar burst fraction. This quantity, correlated to the detector's noise level, is defined by measuring how frequently, in a given run, the PMT counting rate is 20% higher than the baseline level for that run. Then μ_b is obtained by counting the number of events surviving the cuts on Λ and α, and rescaling it to the 1000-second time window.

For each source, Monte-Carlo simulations of all flavor signal events are performed for each data run separately, to account for the different environmental conditions, detector configuration, and performance. Here we assume that the signatures of the signal flux originate from a 10° band centered at the GRB zenith. This choice is justified within this preparatory study as the detector

PoS(ICRC2025)1167

response varies only on angular scales much larger than 5°, and we are only interested in the sensitivity dependence on the source's elevation. The expected number of signal events μ_{sig} in the search region is evaluated by varying the cuts on Λ, and the RoI radius α, which acts on the space angle between the reconstructed muon direction and the parent simulated neutrino direction. The simulated flux from GRBs assumes a single power-law spectrum of E^{-2}, consistent with expectation from standard Fermi-acceleration theory, and $\phi_0 = 10^{-8}$ normalization factor at 1 GeV. Figure 1 shows the distributions of the expected number of background and signal events computed with the dataset relative to GRB150907B, which amounts to 150 days of data taking. As foreseen, more background events are selected toward larger values of α and lower Λ_{cut}. The accepted signal events increase rapidly (and saturate) with the dimension of the search cone, while being constant for varying Λ_{cut}.

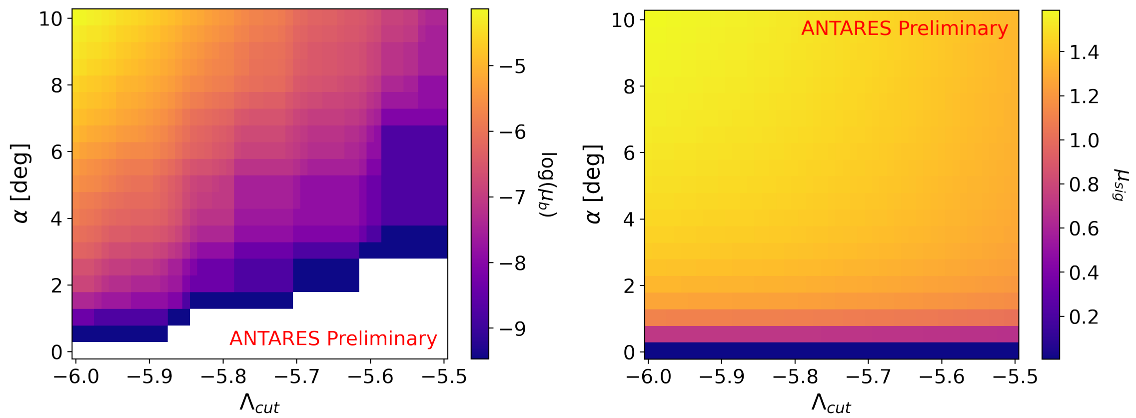

Figure 1: Expected background μ_b (left) and signal μ_{sig} (right) distribution in the RoI and Δt_{GRB}, as function of the Λ_{cut} and search cone radius α, for GRB150907B.

2.2 Search optimization

The obtained $\mu_b(\Lambda_{cut}, \alpha)$ and $\mu_{sig}(\Lambda_{cut}, \alpha)$ distributions are used to compute the values assumed by the test statistic

$$TS(N; \mu_b) = 2 \log \frac{\mathcal{L}_{S+B}(N; \mu_b, \hat{\mu}_{sig})}{\mathcal{L}_B(N; \mu_b)}, \tag{1}$$

where N is the number of observed events, $\mathcal{L}_{S+B}$ and $\mathcal{L}_S$ are the likelihood functions for the Poisson distributed N under the background-only and background-plus-signal hypothesis, respectively. The signal strength value that maximizes $\mathcal{L}_{S+B}$ is denoted by $\hat{\mu}_{sig}$. The distribution of the test statistic is used to evaluate the Model Discovery Potential $\mathcal{MDP}$ here employed to find, for each GRB, the optimal selection to suppress the background and obtain ANTARES sensitivity to the source's signal. The $\mathcal{MDP}$ is defined as

$$\mathcal{MDP} = \frac{\mu_{sig}^{5\sigma}(\mu_b(\Lambda_{cut}, \alpha))}{\mu_{sig}(\Lambda_{cut}, \alpha, \phi = \phi_0 (E/GeV)^{-2})}, \tag{2}$$

where $\mu_{sig}^{5\sigma}$ is the minimum signal strength that leads 50% of the times to a 5σ significant detection, given the background expectation μ_b. The cut on the Λ and α parameters that minimize the

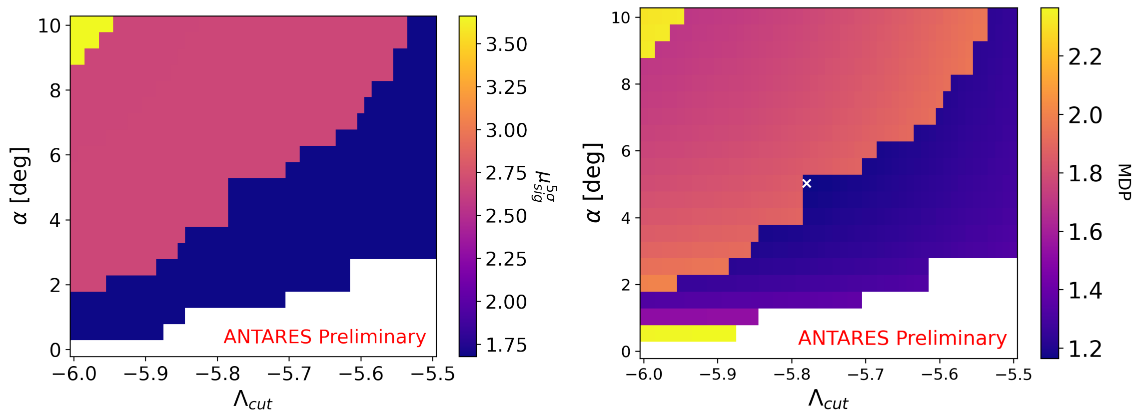

Figure 2: Minimum signal strength $\mu^{5\sigma}_{sig}$ needed for a 5σ significant detection with a 50% probability (left) and $\mathcal{MDP}$ (right), as a function of the Λ_{cut} and α parameters. The event selection optimal point is marked by a white cross and corresponds to the $\mathcal{MDP}$ minimum.

$\mathcal{MDP}$ define our optimal selection for a given GRB. In Figure 2, the obtained values of $\mu^{5\sigma}_{sig}$ for GRB150907B are shown, along with the $\mathcal{MDP}$ distribution and its minimum highlighted by a white cross. The optimal selection of events is found for $\Lambda > \Lambda_{cut} = -5.75$ and $\alpha < 5.03$.

3. GRB classification

GRB phenomenology is extremely rich, with every individual GRB being unique. They are traditionally classified based on their T90 duration, i.e., the time interval during which 90% of the burst's cumulative flux is detected, in "short" (T90<2s) and "long" (T90>2s). These two classes match up (with some outliers [15]) to two different progenitors, respectively, the merger of binary stars and the collapse of a massive star. However, this distinction does not capture the full complexity of GRBs. Additional parameters, such as the spectral hardness or the presence of supernovae, can provide means to further classify them. Examples of different populations are extended emission GRBs, low luminosity GRBs, and choked GRBs. Different classes of GRBs may indicate differences in their underlying physics, with some of them being more likely to have a higher neutrino flux.

In the current analysis, a graph-based clustering (GHCA) algorithm is used to perform a data-driven clustering of GRBs and identify subpopulations of GRBs with similar features [16, 17]. Using this method, four groups of GRBs are extracted from the data, based on the following features: T90, prompt fluence, mean to peak flux, X-ray afterglow flux, spectral index, and initial X-ray temporal decay index. Values for these GRB features are taken from the Fermi GBM and Swift [18] catalogs. No physical interpretation of the subpopulations is attempted at this stage, as the analysis is still in a preliminary phase. This classification is intended to be used in the future to perform population-specific stacking analyses and have more targeted sensitivity estimates, in contrast with the more common approach, where GRBs are stacked together despite their highly variable γ-ray emission and properties.

4. Sensitivity results

With the analysis strategy described above, we obtained an estimate of the sensitivity of the ANTARES detector as a function of the source's zenith. Through the MDP optimization, the best selection cuts $(\Lambda_{cut}^{opt}, \alpha^{opt})$ for each zenith angle between 90° and 180° (up-going sky) are found. Then, pseudo-experiments are generated that randomly draw GRB trigger times t_i and number of observed events $n_{obs} \sim \text{Poisson}(\mu_b(t_i, zen))$. For each pseudo-experiment, we can derive the 90% confidence level (CL) upper limit on the signal flux normalization $\phi_0^{90\%}$

$$\phi_0^{90\%} = \frac{\mu_{sig}^{90\%}(n_{obs}, \mu_b(\Lambda_{cut}^{opt}, \alpha^{opt}))}{\mu_{sig}(\Lambda_{cut}^{opt}, \alpha^{opt}, \phi = \phi_0\ (E/GeV)^{-2})}. \tag{3}$$

In this equation $\mu_{sig}^{90\%}$ is the 90% CL Feldman-Cousin upper limit [19] on the number of signal events given the number of expected background events μ_b at the optimal cuts' values. In Figure 3, it is shown the sensitivity distribution with its median and $\pm 1\sigma$ band (shaded), accounting for the spread in $\phi_0^{90\%}$ values due to the variability introduced by the different trigger times.

In addition, we selected one GRB (in the up-going sky) from each class obtained with the method described in Section 3. The sensitivity of the detector to each of them is also shown.

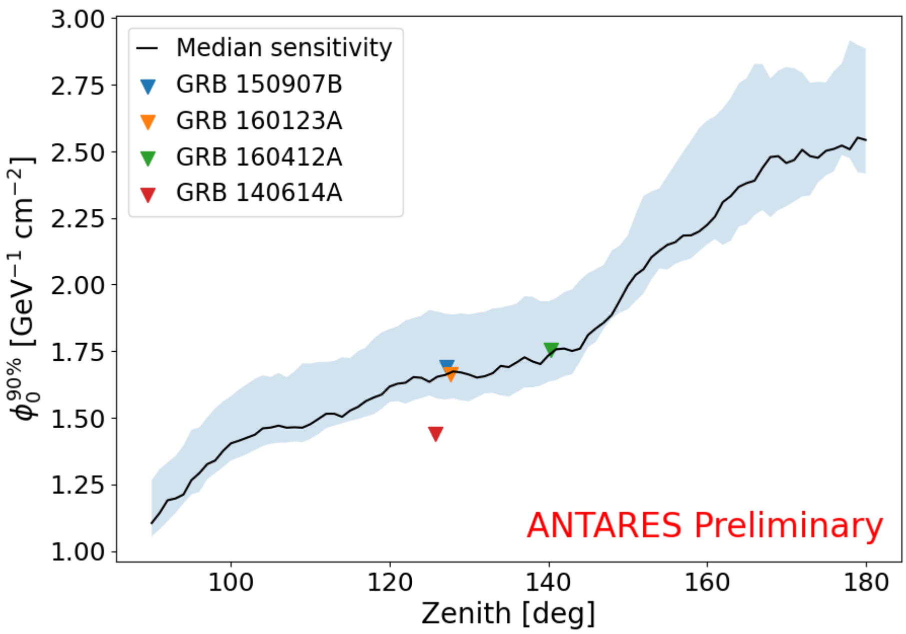

Figure 3: Median sensitivities of ANTARES to a GRB neutrino signal as a function of the source zenith angle, varying between 90° and 180°(i.e., below the local horizon). The $\pm 1\sigma$ region is represented by the shaded band. The sensitivities of the four GRBs belonging to the four groups identified with the method in Section 3 are shown with different colors.

5. Summary and perspectives

This work presents a framework to search for high-energy neutrino emission from Gamma-Ray Bursts using the full ANTARES dataset from 2007 to 2022. The developed time-dependent analysis, focusing on up-going track-like events, searches for the optimal values of the cuts on the track-fit quality parameter Λ and search cone radius α, that minimize the Model Discovery Potential. These values are then used to compute the achievable sensitivity of the ANTARES detector as a function of the source zenith, as seen in Figure 3. Additionally, a data-driven classification of GRBs was implemented to identify subpopulations with potentially different physical properties, laying the basis for targeted population-specific analyses. Future studies will include down-going events and shower-like topologies, extending the accessible sky and neutrino flavors.

This work is part of a larger effort to define the first catalog of Neutrino Energy Distributions for GRBs, analogous to Spectral Energy Distributions (SEDs) in astronomy studies. This project aims to constrain the neutrino spectra of individual GRBs by using combined data from ANTARES, IceCube, and KM3NeT.

References

[1] IceCube Collaboration, *Evidence for high-energy extraterrestrial neutrinos at the icecube detector*, *Science* **342** (2013) 1242856.

[2] KM3NeT Collaboration, *Observation of an ultra-high-energy cosmic neutrino with KM3NeT*, *Nature* **638** (2025) 376.

[3] IceCube, Fermi-LAT, MAGIC, AGILE, ASAS-SN, HAWC, H.E.S.S., INTEGRAL, Kanata, Kiso, Kapteyn, Liverpool Telescope, Subaru, Swift NuSTAR, VERITAS, VLA/17B-403 Collaboration, *Multimessenger observations of a flaring blazar coincident with high-energy neutrino IceCube-170922A*, *Science* **361** (2018) eaat1378 [1807.08816].

[4] IceCube Collaboration, *Evidence for neutrino emission from the nearby active galaxy ngc 1068*, *Science* **378** (2022) 538.

[5] IceCube Collaboration, *Observation of high-energy neutrinos from the galactic plane*, *Science* **380** (2023) 1338.

[6] IceCube Collaboration, *Multi-messenger observations of a binary neutron star merger*, *ApJL* **848** (2017) L12.

[7] S.S. Kimura, *Chapter 9: Neutrinos from Gamma-Ray Bursts*, *The Encyclopedia of Cosmology* **2** (2023) 433 [2202.06480].

[8] ANTARES Collaboration, *ANTARES: the first undersea neutrino telescope*, *Nucl. Instrum. Meth. A* **656** (2011) 11 [1104.1607].

[9] ANTARES Collaboration, *Constraining the contribution of Gamma-Ray Bursts to the high-energy diffuse neutrino flux with 10 yr of ANTARES data*, *Mon. Not. Roy. Astron. Soc.* **500** (2020) 5614 [2008.02127].

[10] IceCube Collaboration, *Searches for Neutrinos from Gamma-Ray Bursts Using the IceCube Neutrino Observatory*, *Astrophys. J.* **939** (2022) 116 [2205.11410].

[11] KM3NeT Collaboration, *Search for neutrino emission from grb 221009a using the km3net arca and orca detectors*, *Journal of Cosmology and Astroparticle Physics* **2024** (2024) 006.

[12] B. Baret et al., *Bounding the Time Delay between High-energy Neutrinos and Gravitational-wave Transients from Gamma-ray Bursts*, *Astropart. Phys.* **35** (2011) 1 [1101.4669].

[13] W.S. Paciesas et al., *The Fourth batse gamma-ray burst catalog (revised)*, *Astrophys. J. Suppl.* **122** (1999) 465 [astro-ph/9903205].

[14] A. von Kienlin et al., *The Fourth Fermi-GBM Gamma-Ray Burst Catalog: A Decade of Data*, *Astrophys. J.* **893** (2020) 46 [2002.11460].

[15] A. Pe'er, *Gamma-Ray Bursts: What Do We Know Today That We Did Not Know 10 Years Ago?*, *Galaxies* **13** (2025) 2 [2412.18681].

[16] K. Kruiswijk and G. de Wasseige, *The classification and categorisation of gamma ray bursts with machine learning techniques for neutrino detection*, *PoS* **ICRC2023** (2023) 1508.

[17] J. Mauro, K. Kruiswijk, E. Moyaux, C. Raab and G. W. de Wasseige, *A Graph-based Hierarchical Clustering Algorithm for population studies of astrophysical objects*, *PoS* **ICRC2025** (these proceedings) 951.

[18] A. Lien et al., *The Third Swift Burst Alert Telescope Gamma-Ray Burst Catalog*, *Astrophys. J.* **829** (2016) 7 [1606.01956].

[19] G.J. Feldman and R.D. Cousins, *A Unified approach to the classical statistical analysis of small signals*, *Phys. Rev. D* **57** (1998) 3873 [physics/9711021].

Full Authors List: The ANTARES Collaboration

A. Albert[a,b], S. Alves[c], M. André[d], M. Ardid[e], S. Ardid[e], J.-J. Aubert[f], J. Aublin[g], B. Baret[g], S. Basa[h], Y. Becherini[g], B. Belhorma[i], F. Benfenati[j,k], V. Bertin[f], S. Biagi[l], J. Boumaaza[m], M. Bouta[n], M.C. Bouwhuis[o], H. Brânzaş[p], R. Bruijn[o,q], J. Brunner[f], J. Busto[f], B. Caiffi[r], D. Calvo[c], S. Campion[s,t], A. Capone[s,t], F. Carenini[j,k], J. Carr[f], V. Carretero[c], T. Cartraud[g], S. Celli[s,t], L. Cerisy[f], M. Chabab[u], R. Cherkaoui El Moursli[m], T. Chiarusi[j], M. Circella[v], J.A.B. Coelho[g], A. Coleiro[g], R. Coniglione[l], P. Coyle[f], A. Creusot[g], A. F. Díaz[w], B. De Martino[f], C. Distefano[l], I. Di Palma[s,t], C. Donzaud[g,x], D. Dornic[f], D. Drouhin[a,b], T. Eberl[y], A. Eddymaoui[m], T. van Eeden[o], D. van Eijk[o], S. El Hedri[g], N. El Khayati[m], A. Enzenhöfer[f], P. Fermani[s,t], G. Ferrara[l], F. Filippini[j,k], L. Fusco[z], S. Gagliardini[s,t], J. García-Méndez[e], C. Gatius Oliver[o], P. Gay[aa,g], N. Geißelbrecht[y], H. Glotin[ab], R. Gozzini[c], R. Gracia Ruiz[y], K. Graf[y], C. Guidi[r,ac], L. Haegel[g], H. van Haren[ad], A.J. Heijboer[o], Y. Hello[ae], L. Hennig[y], J.J. Hernández-Rey[c], J. Hößl[y], F. Huang[f], G. Illuminati[j,k], B. Jisse-Jung[o], M. de Jong[o,af], P. de Jong[o,q], M. Kadler[ag], O. Kalekin[y], U. Katz[y], A. Kouchner[g], I. Kreykenbohm[ah], V. Kulikovskiy[r], R. Lahmann[y], M. Lamoureux[g], A. Lazo[c], D. Lefèvre[ai], E. Leonora[aj], G. Levi[j,k], S. Le Stum[f], S. Loucatos[ak,g], J. Manczak[c], M. Marcelin[h], A. Margiotta[j,k], A. Marinelli[al,am], J.A. Martínez-Mora[e], P. Migliozzi[al], A. Moussa[n], R. Muller[o], S. Navas[an], E. Nezri[h], B. Ó Fearraigh[o], E. Oukacha[g], A.M. Păun[p], G.E. Păvălaş[p], S. Peña-Martínez[g], M. Perrin-Terrin[f], P. Piattelli[l], C. Poirè[z], V. Popa[p], T. Pradier[a], N. Randazzo[aj], D. Real[c], G. Riccobene[l], A. Romanov[r,ac], A. Sánchez Losa[c], A. Saina[c], F. Salesa Greus[c], D. F. E. Samtleben[o,af], M. Sanguineti[r,ac], P. Sapienza[l], F. Schüssler[ak], J. Seneca[o], M. Spurio[j,k], Th. Stolarczyk[ak], M. Taiuti[r,ac], Y. Tayalati[m], B. Vallage[ak,g], G. Vannoye[f], V. Van Elewyck[g,ao], S. Viola[l], D. Vivolo[ap,al], J. Wilms[ah], S. Zavatarelli[r], A. Zegarelli[s,t], J.D. Zornoza[c], J. Zúñiga[c].

[a] Université de Strasbourg, CNRS, IPHC UMR 7178, F-67000 Strasbourg, France
[b] Université de Haute Alsace, F-68100 Mulhouse, France
[c] IFIC - Instituto de Física Corpuscular (CSIC - Universitat de València) c/ Catedrático José Beltrán, 2 E-46980 Paterna, Valencia, Spain
[d] Technical University of Catalonia, Laboratory of Applied Bioacoustics, Rambla Exposició, 08800 Vilanova i la Geltrú, Barcelona, Spain
[e] Institut d'Investigació per a la Gestió Integrada de les Zones Costaneres (IGIC) - Universitat Politècnica de València. C/ Paranimf 1, 46730 Gandia, Spain
[f] Aix Marseille Univ, CNRS/IN2P3, CPPM, Marseille, France
[g] Université Paris Cité, CNRS, Astroparticule et Cosmologie, F-75013 Paris, France
[h] Aix Marseille Univ, CNRS, CNES, LAM, Marseille, France
[i] National Center for Energy Sciences and Nuclear Techniques, B.P.1382, R. P.10001 Rabat, Morocco
[j] INFN - Sezione di Bologna, Viale Berti-Pichat 6/2, 40127 Bologna, Italy
[k] Dipartimento di Fisica e Astronomia dell'Università di Bologna, Viale Berti-Pichat 6/2, 40127, Bologna, Italy
[l] INFN - Laboratori Nazionali del Sud (LNS), Via S. Sofia 62, 95123 Catania, Italy
[m] University Mohammed V in Rabat, Faculty of Sciences, 4 av. Ibn Battouta, B.P. 1014, R.P. 10000 Rabat, Morocco
[n] University Mohammed I, Laboratory of Physics of Matter and Radiations, B.P.717, Oujda 6000, Morocco
[o] Nikhef, Science Park, Amsterdam, The Netherlands
[p] Institute of Space Science - INFLPR subsidiary, 409 Atomistilor Street, Măgurele, Ilfov, 077125 Romania
[q] Universiteit van Amsterdam, Instituut voor Hoge-Energie Fysica, Science Park 105, 1098 XG Amsterdam, The Netherlands
[r] INFN - Sezione di Genova, Via Dodecaneso 33, 16146 Genova, Italy
[s] INFN - Sezione di Roma, P.le Aldo Moro 2, 00185 Roma, Italy
[t] Dipartimento di Fisica dell'Università La Sapienza, P.le Aldo Moro 2, 00185 Roma, Italy
[u] LPHEA, Faculty of Science - Semlali, Cadi Ayyad University, P.O.B. 2390, Marrakech, Morocco.
[v] INFN - Sezione di Bari, Via E. Orabona 4, 70126 Bari, Italy
[w] Department of Computer Architecture and Technology/CITIC, University of Granada, 18071 Granada, Spain
[x] Université Paris-Sud, 91405 Orsay Cedex, France
[y] Friedrich-Alexander-Universität Erlangen-Nürnberg, Erlangen Centre for Astroparticle Physics, Erwin-Rommel-Str. 1, 91058 Erlangen, Germany
[z] Università di Salerno e INFN Gruppo Collegato di Salerno, Dipartimento di Fisica, Via Giovanni Paolo II 132, Fisciano, 84084 Italy
[aa] Laboratoire de Physique Corpusculaire, Clermont Université, Université Blaise Pascal, CNRS/IN2P3, BP 10448, F-63000 Clermont-Ferrand, France
[ab] LIS, UMR Université de Toulon, Aix Marseille Université, CNRS, 83041 Toulon, France
[ac] Dipartimento di Fisica dell'Università, Via Dodecaneso 33, 16146 Genova, Italy
[ad] Royal Netherlands Institute for Sea Research (NIOZ), Landsdiep 4, 1797 SZ 't Horntje (Texel), the Netherlands
[ae] Géoazur, UCA, CNRS, IRD, Observatoire de la Côte d'Azur, Sophia Antipolis, France
[af] Huygens-Kamerlingh Onnes Laboratorium, Universiteit Leiden, The Netherlands
[ag] Institut für Theoretische Physik und Astrophysik, Universität Würzburg, Emil-Fischer Str. 31, 97074 Würzburg, Germany
[ah] Dr. Remeis-Sternwarte and ECAP, Friedrich-Alexander-Universität Erlangen-Nürnberg, Sternwartstr. 7, 96049 Bamberg, Germany
[ai] Mediterranean Institute of Oceanography (MIO), Aix-Marseille University, 13288, Marseille, Cedex 9, France; Université du Sud Toulon-Var, CNRS-INSU/IRD UM 110, 83957, La Garde Cedex, France
[aj] INFN - Sezione di Catania, Via S. Sofia 64, 95123 Catania, Italy
[ak] IRFU, CEA, Université Paris-Saclay, F-91191 Gif-sur-Yvette, France
[al] INFN - Sezione di Napoli, Via Cintia 80126 Napoli, Italy

[am] Dipartimento di Fisica dell'Università Federico II di Napoli, Via Cintia 80126, Napoli, Italy
[an] Dpto. de Física Teórica y del Cosmos & C.A.F.P.E., University of Granada, 18071 Granada, Spain
[ao] Institut Universitaire de France, 75005 Paris, France
[ap] Dipartimento di Matematica e Fisica dell'Università della Campania L. Vanvitelli, Via A. Lincoln, 81100, Caserta, Italy

Acknowledgements

The authors acknowledge the financial support of the funding agencies: Centre National de la Recherche Scientifique (CNRS), Commissariat à l'énergie atomique et aux énergies alternatives (CEA), Commission Européenne (FEDER fund and Marie Curie Program), LabEx UnivEarthS (ANR-10-LABX-0023 and ANR-18-IDEX-0001), Région Alsace (contrat CPER), Région Provence-Alpes-Côte d'Azur, Département du Var and Ville de La Seyne-sur-Mer, France; Bundesministerium für Bildung und Forschung (BMBF), Germany; Istituto Nazionale di Fisica Nucleare (INFN), Italy; Nederlandse organisatie voor Wetenschappelijk Onderzoek (NWO), the Netherlands; Ministry of Education and Scientific Research, Romania; MCIN for PID2021-124591NB-C41, -C42, -C43 and PDC2023-145913-I00 funded by MCIN/AEI/10.13039/501100011033 and by "ERDF A way of making Europe", for ASFAE/2022/014 and ASFAE/2022 /023 with funding from the EU NextGenerationEU (PRTR-C17.I01) and Generalitat Valenciana, for Grant AST22_6.2 with funding from Consejería de Universidad, Investigación e Innovación and Gobierno de España and European Union - NextGenerationEU, for CSIC-INFRA23013 and for CNS2023-144099, Generalitat Valenciana for CIDEGENT/2020/049, CIDEGENT/2021/23, CIDEIG/2023/20, ESGENT2024/24, CIPROM/2023/51, GRISOLIAP/2021/192 and INNVA1/2024/110 (IVACE+i), Spain; Ministry of Higher Education, Scientific Research and Innovation, Morocco, and the Arab Fund for Economic and Social Development, Kuwait. We also acknowledge the technical support of Ifremer, AIM and Foselev Marine for the sea operation and the CC-IN2P3 for the computing facilities.

PoS(ICRC2025)1167